Vibronic transitions from coupled-cluster response theory: Theory and application to HSiF and H_2O

Ove Christiansen
Department of Theoretical Chemistry, Chemical Centre, University of Lund, P.O. Box 124, SE-221 00 Lund, Sweden

Torgeir A. Ruden
San Diego Supercomputer Center, University of California San Diego, La Jolla, California 92093-0505 and Department of Chemistry, University of Oslo, P.O. Box 1033 Blindern, N-0315 Oslo, Norway

Kenneth Ruud[a)]
San Diego Supercomputer Center, University of California San Diego, La Jolla, California 92093-0505

Trygve Helgaker
Department of Chemistry, University of Oslo, P.O. Box 1033 Blindern, N-0315 Oslo, Norway

(Received 14 January 2002; accepted 20 February 2002)

A scheme for calculating the vibrational structure of electronic spectra using coupled-cluster response theory is proposed. To calculate the vibrational structure of electronic transitions, the optimized geometries of the two electronic states, the molecular Hessians, the dipole transition moment and (for vibrationally induced transitions) the geometrical gradient of the dipole transition moment are used in conjunction with a recently developed method for the evaluation of Franck–Condon factors of multidimensional harmonic oscillators. Allowed and vibrationally induced transitions are both described. In this pilot implementation, the required geometrical derivatives are calculated by an automated finite-difference method. The scheme is applied to the $1\,^1A''\leftarrow 1\,^1A'$ transition of monofluorosilylene (HSiF) and the vibrationally induced $1\,^1A_2\leftarrow 1\,^1A_1$ transition of water. © *2002 American Institute of Physics.* [DOI: 10.1063/1.1468639]

I. INTRODUCTION

The importance of the dynamics of electronically excited states for a proper understanding of the appearance of electronic spectra is well established.[1,2] Nevertheless, the theoretical calculation of an electronic spectrum often means just a calculation of the vertical excitation energies, even though the theoretical vertical excitation energy (i.e., the energy difference between two electronic states at the fixed geometry of the ground state) is not an observable. Indeed, the simple vertical spectrum constructed from the calculated vertical excitation energies and their oscillator strengths has little resemblance to the experimentally recorded spectrum.

Occasionally, the term experimental ''vertical'' excitation energy is used to denote the energy of maximum absorption. However, Franck–Condon arguments notwithstanding, this energy cannot be expected to agree well with the theoretical vertical excitation energy. The error made in comparing such ''experimental'' and theoretical vertical excitation energies is quite significant and, with the high quality of modern quantum-chemical techniques, may indeed represent the largest error in the calculations.[3–5] In our opinion, therefore, nuclear motion must be properly taken into account for a meaningful comparison with experiment—at least when aiming for an accuracy of 0.1–0.3 eV, which is typically needed to assign with confidence the features of electronic spectra related to different electronic states. Certainly, the comparison between calculated and experimental 0–0 transition energies (i.e., the excitation energies including zero-point vibrations) is less problematic if this is possible. However, the 0–0 transition energies are not always well-resolved and/or reliably assigned in experimental spectra and they are furthermore not the only type of transition of interest. It is therefore often desirable to consider other transitions or better the overall ''shape'' of the spectrum.

From the previous discussion, it may seem strange that only vertical excitation energies are usually calculated. One reason for this situation is that it is often difficult to address the nuclear motion of the excited state as different molecules and excitation processes require different theoretical treatments. Moreover, even crude descriptions of the nuclear motion require rather elaborate electronic-structure calculations and compromises must therefore be made. In this study, we are concerned with transitions between bound states, noting that excitations between bound and dissociative states require a rather different approach.[1] We combine recent developments for the calculation of excited states employing coupled-cluster response methods;[6,7] numerical geometrical differentiation using automated finite-difference techniques,[8] and multidimensional Franck–Condon factors.[9–11] Although we base our calculations on the use of Franck–Condon fac-

[a)]Permanent address: Department of Chemistry, University of Tromsø, N-9037 Tromsø, Norway.

tors, we note that, in some cases, it may be advantageous to proceed in a different manner.[1,2]

The coupled-cluster methodology is now widely recognized as one of the most accurate *ab initio* methods for calculating ground-state structures and vibrational frequencies.[12,13] Moreover, recent work has established that the coupled-cluster method—through its response-theory generalization—also provides an accurate treatment of excited states. In particular, methods have been developed for systematically improving the accuracy of coupled-cluster response calculations, providing a reasonable degree of control over the error in the calculated excitation energies.[14] A complementary development has been the development of analytical derivative methods for excited-state molecular gradients.[15] By combining these different theoretical developments, 0–0 excitation energies of molecules such as furan,[3] benzene,[6,16] and pyrrole[5] have been calculated to an accuracy better than 0.1 eV—an impressive achievement for systems of this size.

Although the theory of analytical derivatives is well-established, its implementation nevertheless requires a significant programming effort. An easier access to geometrical derivatives is provided by finite-difference methods, which we use here. For our purposes, they have the advantage that the same approach is readily extended to calculations of all the necessary derivatives, that is, to the transition properties as well as to the first and second derivatives of ground- and excited-state total energies. By contrast, their analytical calculation would require an extensive programming effort and, to a large extent, be an independent task for each electronic-structure model. These problems are not shared by the numerical approach, which on the other hand is computationally less efficient than the analytical scheme, although not unconditionally so.[17]

The information generated by the above-mentioned methods can be used in different ways. The focus is here on the calculation of the Franck–Condon factors needed for describing allowed and vibrationally induced transitions. In this work, we use a recently implemented code for calculating Franck–Condon matrix elements for multidimensional harmonic oscillators.[9,11] To our knowledge, such calculations have not yet been been presented at the coupled-cluster level. The calculation of Franck–Condon matrix elements for polyatomic molecules such as benzene using *ab initio* force fields have previously been reported for complete-active-space self-consistent field (CASSCF) wave functions.[10,11]

In Sec. II, we briefly discuss the theory and implementation of our approach for calculating vibronic transitions with coupled-cluster methods. Next, in Sec. III, we present sample calculations for the $1\,^1A'' \leftarrow 1\,^1A'$ transition of silylene HSiF, where new experimental results are available.[18] The vibrationally induced $1\,^1A_2 \leftarrow 1\,^1A_1$ transition in H_2O is discussed in Sec. IV. Section V summarizes our findings.

II. THEORY AND IMPLEMENTATION

A. Vibronic transitions

According to the standard theory, the intensity of a one-photon absorption is related to the square of the dipole matrix element between the initial and final molecular states. In this paper, we invoke this approach to set up scheme for calculating the vibrational structure of transitions between bound electronic states within the Born–Oppenheimer approximation, ignoring the effects of molecular rotation.

Let us write the total wave functions of the two states as products of an electronic wave function $\psi_m(\mathbf{Q};\mathbf{q})$ and a nuclear wave function $\chi_v^m(\mathbf{Q})$, where the electronic and nuclear coordinates are denoted by $\mathbf{q}$ and $\mathbf{Q}$, respectively. We thus seek to calculate the transition dipole moment from the expression,

$$\mathbf{M}_{mn}(v,v') = \langle \psi_m(\mathbf{Q};\mathbf{q})\chi_v^m(\mathbf{Q})|\mu(\mathbf{Q},\mathbf{q})|\psi_n(\mathbf{Q};\mathbf{q})\chi_{v'}^n(\mathbf{Q})\rangle_{\mathbf{Q},\mathbf{q}}, \quad (1)$$

where $\mu(\mathbf{Q};\mathbf{q})$ is the molecular dipole operator and the subscript $\mathbf{Q}$, $\mathbf{q}$ indicates that the integration is carried out over both electronic and nuclear coordinates. Integrating over the electronic coordinates $\mathbf{q}$ first, we may rewrite the transition dipole moment Eq. (1) in the form,

$$\mathbf{M}_{mn}(v,v') = \langle \chi_v^m(\mathbf{Q})|\mu_{mn}(\mathbf{Q})|\chi_{v'}^n(\mathbf{Q})\rangle_{\mathbf{Q}}, \quad (2)$$

where the electronic transition moment $\mu_{mn}(\mathbf{Q})$ between states m and n is a function of the nuclear coordinates,

$$\mu_{mn}(\mathbf{Q}) = \langle \psi_m(\mathbf{Q};\mathbf{q})|\mu(\mathbf{Q},\mathbf{q})|\psi_n(\mathbf{Q};\mathbf{q})\rangle_{\mathbf{q}}. \quad (3)$$

Expanding the electronic transition moment about some reference nuclear configuration $\mathbf{Q}^0$,

$$\mu_{mn}(\mathbf{Q}) = \mu_{mn}(\mathbf{Q}^0) + \sum_i \left.\frac{\partial \mu_{mn}}{\partial Q_i}\right|_{\mathbf{Q}^0} (Q_i - Q_i^0) + \cdots, \quad (4)$$

we arrive at the following expression for the total transition moment:

$$\mathbf{M}_{mn}(v,v') = \mu_{mn}(\mathbf{Q}^0)\langle \chi_v^m(\mathbf{Q})|\chi_{v'}^n(\mathbf{Q})\rangle_{\mathbf{Q}} + \sum_i \left.\frac{\partial \mu_{mn}}{\partial Q_i}\right|_{\mathbf{Q}^0} \langle \chi_v^m(\mathbf{Q})|(Q_i - Q_i^0) \times |\chi_{v'}^n(\mathbf{Q})\rangle_{\mathbf{Q}} + \cdots. \quad (5)$$

In this study, we shall use low-order expansions of this type. However, for this procedure to work, we must first select the reference geometry $\mathbf{Q}^0$. Two natural choices are the equilibrium geometries of either state. We note that, if the results are sensitive to the reference geometry, then the truncated expansion Eq. (5) is probably a poor approximation to Eq. (1).

If $\mu_{mn}(\mathbf{Q}^0) \neq 0$, we speak of an *electronically allowed transition*. To lowest nonzero order in $\mathbf{Q}$, we obtain from Eq. (5) the transition dipole moment,

$$\mathbf{M}_{mn}(v,v') = \mu_{mn}(\mathbf{Q}^0)\langle \chi_v^m(\mathbf{Q})|\chi_{v'}^n(\mathbf{Q})\rangle_{\mathbf{Q}}. \quad (6)$$

In this simple approximation, the total strength of the transition is determined by $\mu_{mn}(\mathbf{Q}^0)$, whereas the vibrational structure arises from the Franck–Condon factors $\langle \chi_v^m(\mathbf{Q})|\chi_{v'}^n(\mathbf{Q})\rangle_{\mathbf{Q}}$. To determine these factors, we need the vibrational wave functions of both electronic states. To calculate the energies and intensities of an allowed transition according to Eq. (6), we must in the harmonic approximation calculate the equilibrium structures of the two electronic states; the molecular Hessians (the harmonic force constants) of both states at their equilibrium geometries; the electronic transition matrix element $\mu_{mn}(\mathbf{Q}^0)$; and the Franck–Condon factors $\langle \chi_v^m(\mathbf{Q})|\chi_{v'}^n(\mathbf{Q})\rangle_{\mathbf{Q}}$ using the normal coordinates obtained from these molecular structures and Hessians. Higher-order corrections may be added if necessary.

When $\mu_{mn}(\mathbf{Q}^0)=0$ because of symmetry, the first term in Eq. (5) vanishes, and we have an *electronically forbidden transition*. Assuming that the next term in the expansion is nonzero, we obtain a *vibrationally induced transition*, whose transition dipole moment is given as

$$\mathbf{M}_{mn}(v,v') = \sum_i \left.\frac{\partial \mu_{mn}}{\partial Q_i}\right|_{\mathbf{Q}^0} \langle \chi_v^m(\mathbf{Q})|(Q_i - Q_i^0)|\chi_{v'}^n(\mathbf{Q})\rangle_{\mathbf{Q}}. \quad (7)$$

To calculate the energies and intensities according Eq. (7), we must in the harmonic approximation calculate the equilibrium structures for the two electronic states; the molecular Hessians of these states at their equilibrium geometries; the gradient of the electronic transition matrix element $\mu_{mn}(\mathbf{Q})$ at $\mathbf{Q}^0$; and the Franck–Condon factors $\langle \chi_v^m(\mathbf{Q})|(Q_i - Q_i^0)|\chi_{v'}^n(\mathbf{Q})\rangle_{\mathbf{Q}}$.

This simple theory is expected to work well for electronic transitions when neither state has a potential-energy surface that is highly anharmonic and when nonadiabatic effects are small. However, it is important to keep in mind that, in many cases, the outlined approach may be inadequate, for example, when there is a symmetry lowering upon excitation, it may be necessary to take into account multiple minima.

B. Calculation of Franck–Condon factors

Our calculation of the multidimensional Franck–Condon factors proceeds by an *LU* decomposition,[9,11]

$$\langle \chi_v^m(\mathbf{Q})|\chi_{v'}^n(\mathbf{Q})\rangle_{\mathbf{Q}} = \langle \chi_0^m(\mathbf{Q})|\chi_0^n(\mathbf{Q})\rangle_{\mathbf{Q}} \sum_{t\leqslant \min(mn)} L_{mt}U_{tn}. \quad (8)$$

The first factor on the right-hand side is an overlap between the two ground-state harmonic oscillators, which is simply obtained from the Gaussian product rule. The *L* and *U* matrix elements of the second factor are obtained by solving recursive equations as described in Ref. 9. This procedure has been implemented in the Mula module,[9,11] developed within the MOLCAS package.[19] For our work, interface routines have been written for exporting the molecular structures, Hessians, and transition dipole gradients calculated by the DALTON program[20] into the Mula module.

C. Finite-difference calculation of Franck–Condon factors

To obtain the molecular equilibrium geometries and harmonic force fields, molecular gradients and Hessians are required for both the ground and the excited state. We here calculate these quantities by numerical differentiation of the energy. Likewise, the geometrical gradient of the electronic transition matrix elements is calculated numerically. The numerical differentiation scheme in Dalton is automated to run the wave function and response parts of the program only for those geometries that are needed to obtain the first and second derivatives of the energy and the properties.

Numerical differentiation usually requires more computational effort than does analytical differentiation. On the other hand, the generality of the numerical technique makes it a useful and flexible tool since it can provide derivatives when no analytical implementation exists. As discussed by Pulay, a combination of numerical and analytical methods often provide the best trade-off between simplicity and efficiency.[21] In passing, we note that, even though numerical methods may be used for the derivatives of the response properties, the response properties themselves can only be calculated analytically, as discussed in the next subsection.

Care has been taken to make the numerical differentiation as general and robust as possible, with minimum loss of efficiency. Since our scheme for numerical differentiation of the total energy has been discussed elsewhere,[8] only its main features are treated here, with emphasis on the differentiation of the transition moments.

We use the standard three-point formula of numerical differentiation.[8,22] Disregarding reductions from symmetry, the number of calculated points scales as N^n, where N is the number of coordinates and n the order of the differentiation. More precisely, the number of points needed is $\Sigma_{i=1}^n 2^i N^i/i!$.

The three-point formula gives derivatives accurate to h^2, where h is the step length and the function value is assumed to be exact to h^{n+2};[8] typically, $10^{-4}\leqslant h\leqslant 10^{-3}$. With the tight convergence criteria used in the calculation of excitation energies and transition moments, the differentiated properties should be accurate to 10^{-6} or better.

The first derivative of the transition moment is obtained by applying the three-point formula to the three Cartesian components μ_α, taking care to select the correct states when the symmetry of the excited state is reduced to that of the distorted geometry, assuming that excited states of the same distorted symmetry do not cross upon distortion. As the distortions are small, this assumption is presumably justified.

The number of points needed for differentiation is reduced by the use of point-group symmetry, differentiating with respect to symmetry-adapted Cartesian coordinates and identifying the nonzero derivatives from the irreducible representations of the coordinates and the operator. Additional reductions are obtained by establishing symmetry relations between the derivative components and geometry points.

In Abelian point-groups, the reductions arise only from relations between points of the same component. These relations may be established by expanding the derivative in a Taylor series and by identifying points that give the same result to order h^{n+2}. For example, for the calculation of the

TABLE I. Vertical excitation energies (ω in eV) and size of transition dipole for the $1\,^1A' \rightarrow 1\,^1A''$ transition in HSiF using an experimental geometry[a] and various basis sets and coupled-cluster models.

	Vertical excitation energy				Size of transition dipole moment[b]			
Model	cc-pVDZ	aug-cc-pVDZ	aug-cc-pVTZ	aug-cc-pVQZ	cc-pVDZ	aug-cc-pVDZ	aug-cc-pVTZ[b]	aug-cc-pVQZ
CCS	3.394	3.297	3.331	3.336	0.7430	0.7016	0.7055	0.7072
CC2	3.249	3.134	3.139	3.135	0.6571	0.6274	0.6307	0.6336
CCSD	3.228	3.115	3.115	3.114	0.6124	0.5850	0.5904	0.5938
CCSDR(3)	3.185	3.072	3.064	3.060				
CC3	3.185	3.073	3.066					

[a]$R_{SiH}=1.528$ Å, $R_{SiF}=1.603$ Å, $\phi(\text{H–Si–F})=96.9$.
[b]At the ground state geometry. At the excited state geometries the corresponding transition dipole moments obtained with the aug-cc-pVTZ basis set are 0.7294, 0.6487, 0.6061 for CCS, CC2, and CCSD, respectively.

component H_{X_i,X_j} of the Hessian with $X_i \notin A_1$, $X_j \notin A_1$, and $X_i \neq X_j$, the following points are equivalent:

$$E(\ldots,X_i+h,\ldots,X_j+h,\ldots)=E(\ldots,X_i-h,\ldots,X_j-h,\ldots), \quad (9)$$

$$E(\ldots,X_i-h,\ldots,X_j+h,\ldots)=E(\ldots,X_i+h,\ldots,X_j-h,\ldots). \quad (10)$$

For a discussion of non-Abelian point groups, see Refs. 8 and 23. Additional reductions are possible by invoking the translational and rotational invariance of the energy.[24] This invariance implies that only $N-M$ Cartesian gradient components are independent, where M is the number of translational and rotational degrees of freedom.

Taking into account these reductions, we need only calculate 7 and 5 energies, respectively, to obtain the gradients of HSiF and H_2O in symmetry-adapted Cartesian coordinates. Likewise, for the Hessians, only 19 and 10 energy calculations are needed. By contrast, for the transition-moment gradient of H_2O, all 18 transition moments must be calculated. However, the derivatives with respect to the totally symmetric coordinates are not needed, reducing the number of points to 12.

D. Coupled-cluster response methods

The coupled-cluster ansatz for the electronic ground-state wave function corresponds to an exponential parameterization in terms of a cluster operator that promotes electrons from a single-determinant Hartree–Fock reference state. The cluster operator itself is written as a sum over individual excitations weighted by the cluster amplitudes—the basic parameters of the coupled-cluster model. The ground-state energy and the equations for the amplitudes are obtained by inserting the coupled-cluster ansatz into the Schrödinger equation and by projecting the resulting equation onto the reference Slater determinant and onto the determinants of excited electronic configurations, respectively.

Approximate coupled-cluster models are established by considering only selected classes of excitations. The popular CCSD model,[25] for example, is obtained by including only single and double excitations in the cluster operator. Other models such as CC2 (Ref. 14) and CC3 (Ref. 26) are obtained by introducing different approximations in the cluster amplitude equations. In this manner, a hierarchy of models (CCS, CC2, CCSD, CC3,...) is established, where higher ac-

TABLE II. Structures (bond lengths in Å and angles in deg) and excitation energies (in eV) for the $1\,^1A' \rightarrow 1\,^1A''$ transition for HSiF predicted using the aug-cc-pVTZ basis set and various coupled-cluster models.

	$1\,^1A'$			$1\,^1A''$			Excitation energies		
	R_{SiH}	R_{SiF}	⟨HSiF⟩	R_{SiH}	R_{SiF}	⟨HSiF⟩	Vert.[a]	Adia.[b]	0–0
CCS	1.522	1.596	96.9	1.507	1.589	114.9	3.331	3.159	3.141
CC2	1.527	1.636	96.2	1.517	1.632	115.6	3.142	2.993	2.970
CCSD	1.531	1.620	96.5	1.527	1.614	115.2	3.115	2.972	2.946
Triples corr. (CC3-CCSD/aT vert.)									−0.049
Basis set corr. [CCSDR(3)/aQ-aT vert.]									−0.004
Final estimate									2.893
Expt. R_e[c]	1.528(5)	1.603(3)	96.9(5)	1.526(14)	1.597(3)	115.0(6)			
Expt.[d]	(1.530)	1.605	97.0	(1.484)	1.609	111.0			
Expt.[e]	1.534	1.604	(97.6)	1.543	1.599	(115.3)			
Expt.[f]				1.548	1.602	(114.5)			2.884
Previous calc.	1.521	1.618	97.1	1.571	1.607	114.5			

[a]Vert. is at the ground state geometry optimized for the particular model.
[b]Adia. is the energy difference between the minima in the two states obtained within the Born–Oppenheimer approximation.
[c]Reference 18.
[d]Reference 37.
[e]Reference 38.
[f]Reference 35.

TABLE III. Calculated harmonic vibrational frequencies (in cm^{-1}) for the $1\,^1A'$ and $1\,^1A''$ states of HSiF predicted using CCS CC2, CCSD, and an aug-cc-pVTZ basis set. Experimental vibrational frequencies are also included (both fundamentals and estimated harmonic).

	$1\,^1A'$			$1\,^1A''$		
	ν_1 Si–H str.	ν_2 bend	ν_3 Si–F str.	ν_1 Si–H str.	ν_2 bend	ν_3 Si–F str.
CCS	2095	936	892	2043	676	917
CC2	2046	870	808	1941	589	815
CCSD	2015	877	847	1845	596	863
Expt. est. harm.[a]				1816	597	867
Expt. est. harm. fit.[a]	1977	861	834	1836	590	871
Expt. fund.[a]				1547	563	862
Expt. fund.[b]				1547	558	857
Expt.[c]		860				
Expt. matrix[d]	1913.1	859.0	833.7			
Previous calc.[e]	2083	929	849	1544	570	865

[a]Reference 18.
[b]Reference 35.
[c]Reference 39.
[d]Reference 40.
[e]Previous calc: CCSD/TZ($2df$,$2dp$) for the ground state. MRCI/TZ($2df$,$2dp$) for excited state. Gregory and Grev, as cited in Ref. 18.

curacy is obtained by going to higher levels in the hierarchy.

Although well-suited to the molecular ground state, this procedure cannot in general be applied to excited states since these can rarely be represented by a single-determinant Hartree–Fock reference state. Excited electronic states can nevertheless be described by means of coupled-cluster response theory. In response theory, the electronic spectrum (including the electronic transition properties) is defined for any quantum-chemical approximation once the ground-state model is given.[27,28] In this manner, coupled-cluster theory can also be used for excited states, as the single-reference restriction applies only to the ground state.

Expressions for the calculation of excitation energies and transition matrix elements by response theory are discussed elsewhere. We here use the implementation in the local version of DALTON (Ref. 20) described in Refs. 6 and 7 for excitation energies and transition dipole moments, respectively. Excitation processes may be studied by a number methods, including CCS, CC2, CCSD, and CC3 for both ground and excited states. We also use the CCSDR(3) method,[29] involving a CC(3) calculation for the ground state.[30] In passing, we note that the popular CCSD(T) method can in general not be used for excited states.

III. COMPUTATIONAL DETAILS

All HSiF calculations invoke the frozen-core approximation, where the Hartree–Fock orbitals corresponding to the

TABLE IV. Vibrational structure in the $1\,^1A' \rightarrow 1\,^1A''$ transition for HSiF from experiment (Ref. 18) and coupled-cluster calculations with an aug-cc-pVTZ basis set. Energies (in cm^{-1}) are given relative to the 0–0 transition energy (Expt. at 23 260.021 cm^{-1}), numbering of modes as in Table III. See text for discussion of assignments.

	Expt.		CCS		CC2		CCSD	
Assignment[a]	Rel.E.	Int.	Rel.E	Int.	Rel.E	Int.	Rel.E	Int.
0_0^0	0.0	*m*	0	0.65×10^{6}	0	0.49×10^{6}	0	0.55×10^{6}
2_0^1	558.4	*m*	676	0.20×10^{7}	587	0.15×10^{7}	596	0.17×10^{7}
3_0^1	856.5	*vw*	917	0.74×10^{4}	815	0.59×10^{4}	863	0.43×10^{4}
2_0^2	1106.0	*s*	1351	0.25×10^{7}	1175	0.22×10^{7}	1191	0.21×10^{7}
$2_0^1 3_0^1$	1411.2	*vw*	1593	0.22×10^{5}	1402	0.19×10^{5}	1458	0.13×10^{5}
1_0^1	1546.9	*m*	2043	0.15×10^{4}	1941	0.17×10^{3}	1844	0.74×10^{3}
2_0^3	1641.1	*m*	2027	0.19×10^{7}	1762	0.16×10^{7}	1787	0.15×10^{7}
3_0^2?	1703.6	*vw*	1843	0.24×10^{3}	1630	0.77×10^{2}	1726	0.98×10^{2}
$2_0^2 3_0^1$	1945.2	*w*	2268	0.29×10^{5}	1989	0.25×10^{5}	2054	0.17×10^{5}
$2_0^1 3_0^2$			2509	0.72×10^{3}	2217	0.24×10^{3}	2321	0.30×10^{3}
$1_0^1 2_0^1$	2038.7	*m*	2719	0.30×10^{4}	2528	0.12×10^{3}	2439	0.39×10^{4}
2_0^4	2160.5	*m*	2702	0.82×10^{6}	2349	0.73×10^{6}	2382	0.60×10^{6}
1_0^3			2751	0.42×10^{0}	2444	0.83×10^{0}	2589	0.12×10^{1}
$1_0^1 3_0^1$	2398.2	*m*	2960	0.39×10^{0}	2756	0.46×10^{1}	2706	0.56×10^{2}
$2_0^3 3_0^1$?	2496.7	*vw*	2944	0.22×10^{5}	2577	0.19×10^{5}	2650	0.12×10^{5}

[a]Question marks refer to question marks in the original assignments in Ref. 18.

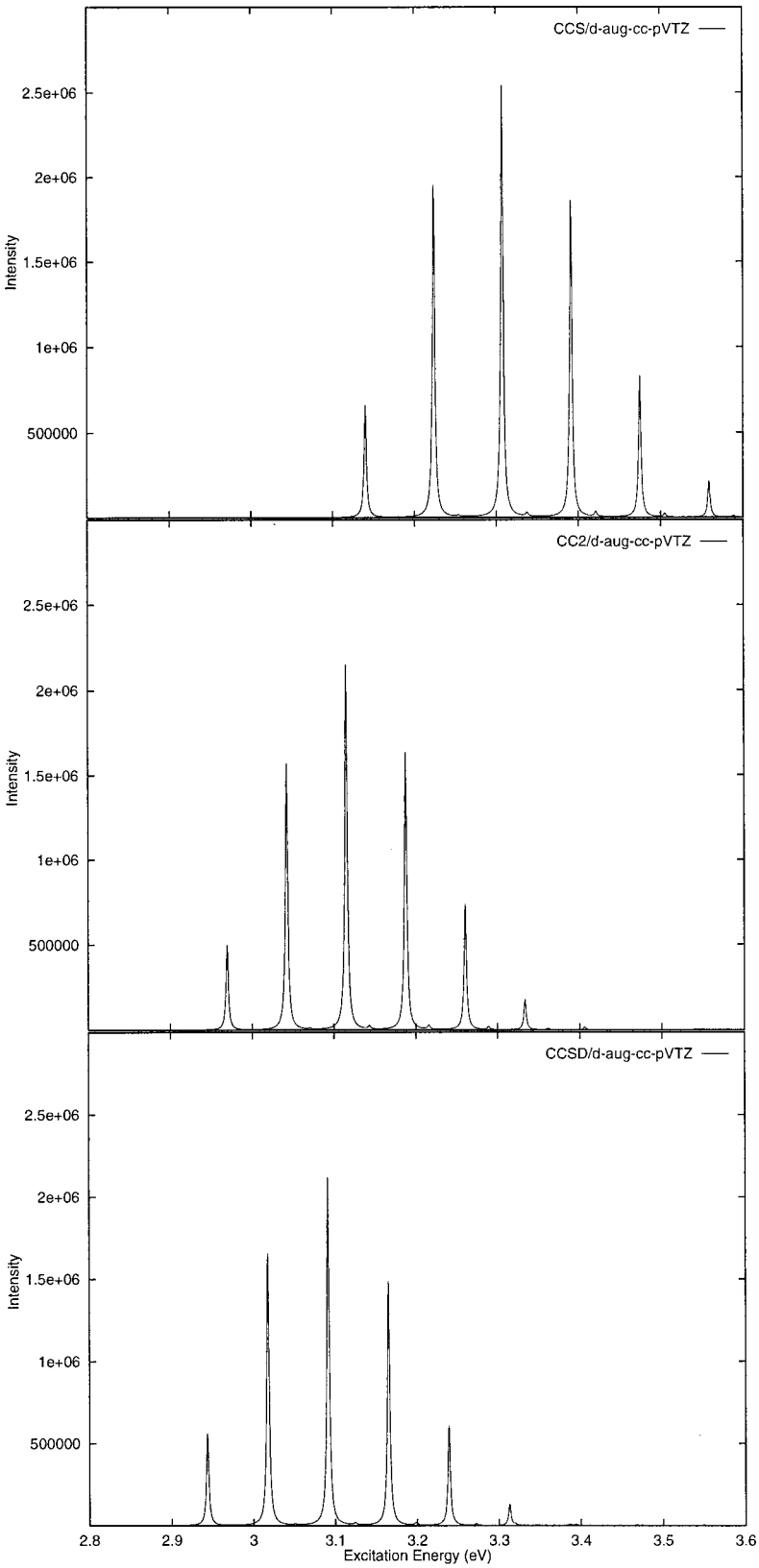

FIG. 1. The $1\,^1A''\leftarrow 1\,^1A'$ spectrum (intensities in arbitrary units as function of energy in eV) of HSiF as predicted in CCS, CC2, and CCSD using the aug-cc-pVTZ basis set and the harmonic approximation.

F $1s$ and the Si $1s2s2p$ core orbitals are frozen in the coupled-cluster calculations. In the initial, exploratory studies of electron correlation and basis-set effects on the $1\,^1A'\leftarrow 1\,^1A'$ transition of HSiF, we use the recently determined experimental ground-state geometry[18] and the correlation-consistent basis sets cc-pVDZ and aug-cc-pVXZ.[31,32] In the subsequent optimizations and force-constant calculations, we used the aug-cc-pVTZ basis. In the water calculations, we used the d-aug-cc-pVTZ basis set, with the Hartree–Fock orbital corresponding to the oxygen $1s$ orbital frozen.

TABLE V. The $1\,^1A_2 \rightarrow 1\,^1A_1$ transition for H_2O as obtained in CCSD/d-aug-cc-pVTZ calculations. Bond length in Å, angles in deg, excitation energies in eV, vibrational frequencies in cm^{-1}.

	R_{OH}	Angle	Vert.	Adia.	0–0	ω_{A_1}	ω_{A_1}	ω_{B_1}
CCS								
$1\,^1A_1$	0.9410	106.3				1591	4090	4242
$1\,^1A_2$	1.0798	101.8	10.462	10.129	9.976	1254	2093	4116
CC2								
$1\,^1A_1$	0.9634	103.9				1625	3786	3914
$1\,^1A_2$	1.0670	105.7	8.844	8.542	8.354	1255	2337	2706
CCSD								
$1\,^1A_1$	0.9589	104.4				1662	3849	3955
$1\,^1A_2$	1.0944	101.9	9.347	9.023	8.801	1003	1963	2924
CCSDR(3)								
$1\,^1A_1$	0.9617	104.2				1647	3810	3919
$1\,^1A_2$	1.1879	94.8	9.346	8.926	8.716	829	1658	3508
CC3								
$1\,^1A_1$	0.9620	104.1				1646	3806	3915
$1\,^1A_2$	1.2003	94.1	9.350	8.913	8.709	840	1628	3612

Transition matrix elements have only been implemented for the CCS, CC2, and CCSD methods; in the CC3 vibrational structure calculations, the CCSD transition dipoles have been used instead.

IV. RESULTS

A. The $1\,^1A'' \leftarrow 1\,^1A'$ transition in HSiF

We first studied the $1\,^1A'' \leftarrow 1\,^1A'$ vertical excitation energy and transition dipole moment at the experimental geometry, using a series of basis sets and computational models (see Table I). The variations in the vertical excitation energy in the sequence CCS–CC2–CCSD–CCSDR(3)–CC3 is small. In particular, the effect of including triple excitations—that is, the difference between CCSDR(3) or CC3 and CCSD—is about -0.05 eV. The error in the vertical excitation energies is reduced by about a factor of 3 going from CCSD to CC3, and the remaining correlation effects are probably quite small. Similarly, the basis-set effects are small, in particular, the difference between the aug-cc-pVTZ and the aug-cc-pVQZ results is only a few thousandths of an eV.

Based on these observations, we expect to predict the vertical energy difference to an accuracy of a few hundredths of an eV. At the experimental geometry, our best estimate is 3.06 eV, as obtained at the CCSDR(3)/aug-cc-pVQZ level. The CC3 − CCSDR(3) difference is about only 0.002 eV (aug-cc-pVTZ) and does not change this estimate. For the transition dipole moment, diffuse basis functions are more important. There is also a difference of a few percent between CC2 and CCSD, which is the accuracy we shall assume for the CCSD transition dipole moment.

The aug-cc-pVTZ basis thus gives a satisfactory description of the vertical excitation. It is well-known that basis sets of polarized triple-zeta quality are adequate for correlated calculations of molecular structures and vibrations,[12,33] although larger sets are needed for results close to the basis-set limit. In the following, we shall use the aug-cc-pVTZ basis as a compromise between cost and accuracy.

In Table II, we have listed the ground- and excited-state structures optimized using the CCS, CC2, and CCSD models in the aug-cc-pVTZ basis. Included here are also the experimental structures, only one of which is an R_e structure. There is a satisfactory agreement between the CCSD geometry and the recent experimental R_e structure of Harper *et al.*[18] For R_{SiH} and the bond angle, there is an almost perfect agreement; for R_{SiF}, the discrepancy is less than 0.02 Å, in accordance with the accuracy that can be expected for the CCSD model, in particular in the frozen-core approximation.[12,34]

From the energies at the optimized structures, we obtain an adiabatic excitation energy 0.15 eV below the vertical excitation energy; zero-point vibrations lower the excitation energy further. The final CCSD/aug-cc-pVTZ 0–0 excitation energy is 2.946 eV. Including the corrections for triples excitations and basis-set incompleteness found for the vertical energies, we obtain 2.893 eV, compared with 2.884 eV from experiment.[35] The small discrepancy of 0.009 eV is well within the expected error bars of our calculations, as discussed for the vertical excitation above.

In Table III, we have listed the harmonic vibrational frequencies calculated with the CCS, CC2, and CCSD models in the aug-cc-pVTZ basis, in addition to some experimental results. The agreement with the estimated harmonic frequencies of Harper *et al.*[18] is acceptable, noting that an error of about 20 cm^{-1} is to be expected for harmonic frequencies at the CCSD level. The discrepancy is somewhat larger for the Si–H stretching mode, but this may arise from a larger uncertainty in the extraction of the harmonic frequency from the fundamental. The calculations correctly predict the reduction in the frequency of Si–H stretching and bending modes as well as the slight increase in the Si–F stretching frequency upon electronic excitation.

In the calculation of the Franck–Condon factors, a reference structure must be chosen. In this context, the absolute electronic transition dipole becomes a simple constant [see Eq. (6)]. From Table I, we note a discrepancy of a few percent between the transition dipoles at the equilibrium geometry of the ground and excited states. Combined with the previously discussed uncertainty in the transition dipole mo-

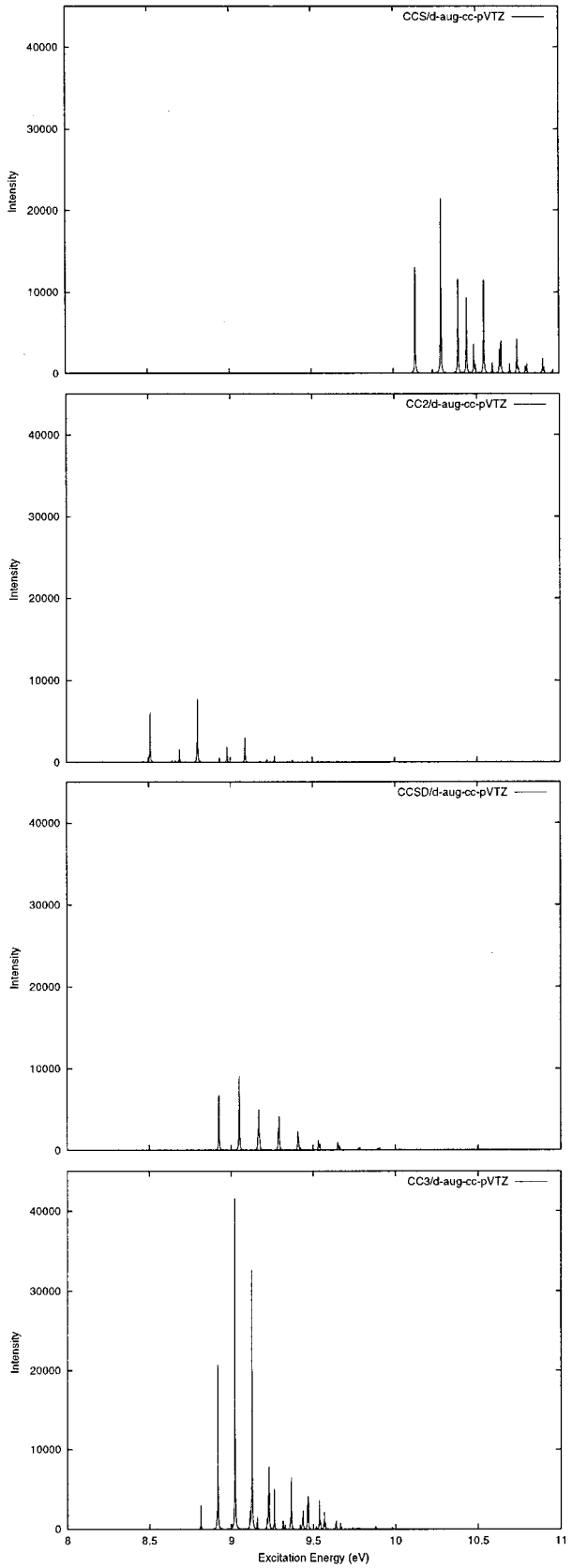

FIG. 2. The $1\,^1A_2 \leftarrow 1\,^1A_1$ spectrum (intensities in arbitrary units as function of energy in eV) of H_2O as predicted in CCS, CC2, CCSD, and CC3 approximations using the d-aug-cc-pVTZ basis set and the harmonic approximation.

ment of the same magnitude, this difference gives a total uncertainty in the predicted transition probability of 4%–5%. Nevertheless, the shape of the spectrum, that is, the relative size of the peaks, is determined mainly by the molecular structure and the normal coordinates. Thus, there is reason to believe that a reasonable accuracy in the structure and harmonic frequencies ensures an accurate prediction of the spectrum.

The calculated intensities are given in Table IV and the corresponding simulated spectra are depicted in Fig. 1. Table IV includes excitations corresponding to CCSD excitation energies less than 2800 cm^{-1} above the 0–0 excitation energy. The results of the experiments by Harper *et al.*[18] are included for comparison. In the simulated spectra, the vibronic transitions have been given a Lorentzian width, introduced to make the features of the spectrum more easily recognizable.

The calculated Franck–Condon factors agree well with the stronger patterns found experimentally. In particular, in agreement with experiment, the 2_0^2 transition is the strongest, followed by 2_0^1 and 2_0^3 and then by 0_0^0 and 2_0^4. The stronger transition within each pair is more difficult to predict.

Another prediction is that the 3_0^n progression is significantly weaker, lending support to some of the experimental assignments of Harper *et al.*[18] and the experimentally derived value for the excited-state frequency. Further support is obtained from the observation that, unlike for the other modes, theory and experiment both predict an increase in the frequency of this mode upon electronic excitation.

Still, there are aspects of the weaker features where the calculated intensity pattern does not match the experimental results, such as the relative strengths of the transitions involving the ν_3 mode relative to the ν_1 mode. This may indeed reflect a problem with the calculations, in particular, as we go to higher energies, the harmonic approximation is expected to become less adequate. Also, the errors in structures and frequencies may have some effect on the calculated transition strengths. On the other hand, there are also uncertainties in the experimental assignments of these weaker features, as indicated by question marks in the table. However, even though some reassignments would improve the agreement with the calculated intensity patterns, the limitations of our calculations make it difficult to be conclusive about such reassignments.

B. The $1\,^1A_2 \leftarrow 1\,^1A_1$ vibrationally-induced transition in water

As an example of vibrationally induced transitions, we consider the $1\,^1A_2 \leftarrow 1\,^1A_1$ transition in water. To our knowledge, this transition has not yet been assigned experimentally, probably because it lies in the low-energy tail of the much stronger and very broad $\tilde{B}$ band (the optically allowed $2\,^1A_1 \leftarrow 1\,^1A_1$ transition). The structure of the spectrum in this region (around 9.4 eV) appears to be dominated by the photodissociation of the $\tilde{B}$ state. Nevertheless, we shall go ahead and investigate the structure of the absorption due to the $1\,^1A_2 \leftarrow 1\,^1A_1$ excitation.

The effects of basis set and correlation level in coupled-

cluster calculations on the lowest excited states of water have been discussed previously.[36] The CC3/d-aug-cc-pVTZ vertical excitation energy of 9.35 eV should be accurate to within 0.1 eV. The calculated structures, harmonic frequencies, and excitation energies are listed in Table V and the calculated spectra are depicted in Fig. 2.

The excited state appears to have a significantly longer bond length and a smaller bond angle than the ground state. However, there is some variation among the different models and triples appear to be important, in particular for the bond angle. For all models, the vibrational frequencies are reduced drastically upon electronic excitation. Our best estimate of the 0–0 excitation energy is 8.71 eV, obtained with the CC3/d-aug-cc-pVTZ model, that is, 0.64 eV lower than the vertical excitation energy. In the CC3 calculations, the strongest vibronic transitions are due to a progression in the 840 cm^{-1} excited state frequency, with a maximum at $n=3$. Because of the large differences among the predicted structures, the spectra are different for the different coupled-cluster models. The significantly larger intensity of CC3 compared with the simpler methods probably arises from the larger changes in the bond angle for CC3 and the accompanying effect on the bending vibrational mode.

The largest vibronic oscillator strength is less than 1×10^{-4}. For comparison, the vertical electronic oscillator strength of the close-lying $\tilde{B}$ state is about 0.5.

V. SUMMARY

We have presented a scheme for calculating vibronic spectra that combines coupled-cluster response theory, automated numerical differentation, and the calculation of multidimensional Franck–Condon factors. Sample calculations have been presented for the $1\,^1A''\leftarrow1\,^1A'$ transition in monofluorosilylene (HSiF) and for the vibrationally induced $1\,^1A_2\leftarrow1\,^1A_1$ transition of water.

The strategy employed leads to a knowledge about the equilibrium structures and harmonic vibrations of both electronic states and converts that information into a ''spectrum'' by means of a Franck–Condon analysis, providing an illustrative link between the raw electronic-structure data and the experimentally observed spectrum. In this way, not just the 0–0 transition energy but the whole ''shape'' of the spectrum can be compared, thereby aiding the comparison between theory and experiment and assisting the assignments of the experimental spectrum.

ACKNOWLEDGMENTS

The authors would like to acknowledge useful discussions with P. R. Taylor. O.C. acknowledges support by the Swedish Natural Science Research Council (NFR). They are grateful to P.-Å. Malmqvist and N. Forsberg for access to and help in using the Mula program. K.R. has been supported by the Norwegian Research Council through a postdoctoral fellowship (Grant No. 125851/410) and through a grant of computer time from the Program for Supercomputing.

[1] R. Schinker, *Photodissociation Dynamics* (Cambridge University Press, Cambridge, 1993).
[2] H. Höppel, W. Domcke, and L. S. Cederbaum, Adv. Chem. Phys. **57**, 59 (1984).
[3] O. Christiansen and P. Jørgensen, J. Am. Chem. Soc. **120**, 3423 (1998).
[4] E. R. Davidson and A. A. Jarzecki, Chem. Phys. Lett. **285**, 155 (1998).
[5] O. Christiansen, J. Gauss, P. Jørgensen, and J. F. Stanton, J. Chem. Phys. **111**, 525 (1999).
[6] O. Christiansen, H. Koch, A. Halkier, P. Jørgensen, T. Helgaker, and A. Sanchez de Meras, J. Chem. Phys. **105**, 6921 (1996).
[7] O. Christiansen, A. Halkier, H. Koch, P. Jørgensen, and T. Helgaker, J. Chem. Phys. **108**, 2801 (1998).
[8] T. A. Ruden, P. Taylor, and T. Helgaker (unpublished).
[9] P.-Å. Malmqvist and N. Forsberg, Chem. Phys. **228**, 227 (1998).
[10] A. Cesar, H. Ågren, T. Helgaker, P. Jørgensen, and H. J. Aa. Jensen, J. Chem. Phys. **95**, 5906 (1991).
[11] A. Bernhardsson, N. Forsberg, P.-Å. Malmqvist, B. O. Roos, and L. Serrano-Andres, J. Chem. Phys. **112**, 2798 (2000).
[12] T. Helgaker, P. Jørgensen, and J. Olsen, *Molecular Electronic-Structure Theory* (Wiley, Chichester, 2000).
[13] D. Feller and D. A. Dixon, J. Chem. Phys. **115**, 3484 (2001).
[14] O. Christiansen, H. Koch, and P. Jørgensen, Chem. Phys. Lett. **243**, 409 (1995).
[15] J. F. Stanton and J. Gauss, Theor. Chim. Acta **91**, 267 (1995).
[16] O. Christiansen, J. F. Stanton, and J. Gauss, J. Chem. Phys. **108**, 3987 (1998).
[17] J. Breidung, W. Thiel, J. Gauss, J. F. Stanton, J. Chem. Phys. **110**, 3687 (1999).
[18] W. W. Harper, D. A. Hostutler, and D. J. Clouthier, J. Chem. Phys. **106**, 4367 (1997).
[19] MOLCAS, Version 5, K. Andersson, M. Barysz, A. Bernhardsson *et al.* (Lund University, Sweden, 2000).
[20] DALTON, a molecular electronic structure program, Release 1.2 (2001), written by T. Helgaker, H. J. Aa. Jensen, P. Jørgensen *et al.*
[21] P. Pulay, in *Modern Electronic Structure Theory, Part II*, edited by D. R. Yarkony (World Scientific, Singapore, 1995).
[22] L. Råde and B. Westergren, *Beta, Mathematics Handbook* (Studentlitteratur, Lund, 1999).
[23] J. F. Stanton, Int. J. Quantum Chem. **106**, 19 (1991).
[24] T. Helgaker, Acta Chem. Scand., Ser. A **A42**, 515 (1988).
[25] G. D. Purvis and R. J. Bartlett, J. Chem. Phys. **76**, 1910 (1982).
[26] O. Christiansen, H. Koch, and P. Jørgensen, J. Chem. Phys. **103**, 7429 (1995).
[27] J. Olsen and P. Jørgensen, in *Modern Electronic Structure Theory, Part I*, edited by D. R. Yarkony (World Scientific, Singapore, 1995).
[28] O. Christiansen, P. Jørgensen, and C. Hättig, Int. J. Quantum Chem. **68**, 1 (1998), and references therein.
[29] O. Christiansen, H. Koch, and P. Jørgensen, J. Chem. Phys. **105**, 1451 (1996).
[30] H. Larsen, J. Olsen, P. Jørgensen, and O. Christiansen, J. Chem. Phys. **113**, 6677 (2000); **114**, 10985(E) (2001).
[31] T. H. Dunning, J. Chem. Phys. **90**, 1007 (1989).
[32] R. A. Kendall, T. H. Dunning, and R. J. Harrison, J. Chem. Phys. **96**, 6796 (1992).
[33] J. M. L. Martin, J. Chem. Phys. **100**, 8186 (1994).
[34] T. Helgaker, J. Gauss, P. Jørgensen, and J. Olsen, J. Chem. Phys. **106**, 6430 (1997).
[35] W. W. Harper, J. Karolzcak, D. J. Clouthier, and S. C. Ross, J. Chem. Phys. **103**, 883 (1995).
[36] O. Christiansen, T. Nymand, and K. V. Mikkelsen, J. Chem. Phys. **113**, 8101 (2000).
[37] T. Suzuki and E. Hirota, J. Chem. Phys. **85**, 5541 (1986).
[38] R. N. Dizon and N. G. Wright, Chem. Phys. Lett. **117**, 280 (1985).
[39] H. U. Lee and J. P. Deneufville, Chem. Phys. Lett. **99**, 394 (1983).
[40] Z. K. Ismail, L. Fredin, R. H. Hauge, and J. L. Margrave, J. Chem. Phys. **77**, 1626 (1982).